Published in final edited form as:
Osteoarthritis Cartilage. 2010 October ; 18(10): 1291–1299. doi:10.1016/j.joca.2010.05.020.

Meniscus and Cartilage Exhibit Distinct Intra-Tissue Strain Distributions Under Unconfined Compression

Janice H. Lai, M.S. and **Marc E. Levenston, Ph.D.**[*,1]
[*] Department of Mechanical Engineering, Stanford University, Stanford, CA 94305-4038

Abstract

Objective—To examine the functional behavior of the surface layer of the meniscus by investigating depth-varying compressive strains during unconfined compression.

Design—Pairs of meniscus and articular cartilage explants (n=12) site-matched at the tibial surfaces were subjected to equilibrium unconfined compression at 5, 10, 15, and 20% compression under fluorescence imaging. Two-dimensional deformations were tracked using digital image correlation. For each specimen, local compressive engineering strains were determined in 200μm layers through the depth of the tissue. In samples with sharp strain transitions, bi-linear regressions were used to characterize the surface and interior tissue compressive responses.

Results—Meniscus and cartilage exhibited distinct depth-dependent strain profiles during unconfined compression. All cartilage explants had elevated compressive engineering strains near the surface, consistent with previous reports. In contrast, half of the meniscus explants tested had substantially stiffer surface layers, as indicated by surface engineering strains that were ~20% of the applied compression. In the remaining samples, surface and interior engineering strains were comparable. Two-dimensional Green's strain maps revealed highly heterogeneous compressive and shear strains throughout the meniscus explants. In cartilage, the maximum shear strain appeared to be localized at 100–250μm beneath the articular surface.

Conclusions—Meniscus was characterized by highly heterogeneous strains during compression. In contrast to cartilage, which consistently had a compliant surface region, meniscal explants were either substantially stiffer near the surface or had comparable compressive stiffness through the depth. The relatively compliant interior may allow the meniscus to maintain a consistent surface contour while deforming during physiologic loading.

Keywords

Meniscus; cartilage; strain mapping; compression; tissue mechanics

[1]Correspondence to: Marc E. Levenston, Ph.D., Department of Mechanical Engineering, 233 Durand Building, Stanford University, Stanford, CA 94305-4038, 650.723.9464 (P), 650.725.1587 (F), levenston@stanford.edu.

AUTHOR CONTRIBUTIONS

JL and ML participated in the conception and design of the study, data analysis and interpretation, and drafting and revision of the manuscript. ML supervised the study and JL performed the experiments and acquired data.

CONFLICT OF INTEREST

The authors have no conflict of interest to declare.

INTRODUCTION

Articular cartilage and meniscus play crucial roles in load bearing and load distribution, providing stability as well as lubrication during movement of the knee joint. The biomechanical functions of cartilage and meniscus are strongly dependent on tissue geometry, ultrastructure, and composition. In an osteoarthritic knee, degradation of cartilage and meniscus involves alterations in biochemical composition, leading to compromised mechanical function and altered load transfer within the joint[1]. These changes in load distribution can in turn induce further degeneration of the tissues in the knee joint and accelerate disease progression[2]. Understanding the structure-function relationships in normal tissue provides valuable baseline information to elucidate the roles of tissue level mechanical changes in the initiation and progression of degenerative joint disease.

Both the ultrastructure and biochemical composition vary significantly throughout the tissue in both cartilage and meniscus[1,3], contributing to variations in mechanical properties and conferring specific mechanical functions. In the superficial zone of articular cartilage, the relatively low proteoglycan (PG) content and high water content lead to a relatively low compressive modulus, while the dense collagen fibrils oriented parallel to the articular surface contribute to a high in-plane tensile modulus in the surface region[4]. The combination of a relatively high PG content and a low water content results in a higher compressive modulus in the middle zone[5]. In meniscus, the superficial zone is characterized by a fine mesh of randomly oriented collagen fibrils lying above a lamellar layer of collagen fibril bundles[6], while the interior of the tissue consists of bundles of circumferentially oriented collagen I fibers surrounded by a secondary network composed of multiple collagen types and PGs[7–10]. The circumferentially oriented collagen fibers are responsible for sustaining high tensile hoop stresses due to compression and extrusion of the meniscus, and the density, orientation and distribution of the circumferential fibers strongly influences the macroscopic tensile, compressive and shear responses[3,11–13].

Image-based techniques involving digital image correlation and related texture analysis procedures have provided valuable insights into the spatially varying mechanical properties of articular cartilage. Studies examining depth-varying strain distributions in cartilage during both unconfined and confined compression have shown that the surface region experienced significantly higher compressive strain compared to the rest of the tissue. Schinagl et al.[14] found that the compressive modulus increased 15-fold over the first 1mm beneath the articular surface in mature bovine patellofemoral groove cartilage. This progressive increase in compressive modulus with depth has been observed consistently in articular cartilage from different joints, species and ages[14–19]. These techniques have been extended to examine cartilage mechanics in a variety of other situations, including strain fields surrounding indenters[20] and cartilage defects[21,22], relationships between macroscopic strain and chondron deformation[23], compression of cross-sections of intact joints[18,24], and shear properties under static, dynamic and sliding conditions[25–28]. In contrast, few studies have similarly focused on the details of fibrocartilage tissue mechanics. Image analysis techniques have been used to examine strain fields in rat intervertebral disc under compression[29] and in bovine annulus fibrosus under dynamic shear [30]. Upton et al. [31] used texture analysis to determine macroscale strain distributions in meniscus samples under tension for comparison to cell level deformations. Overall, however, relatively little is known about the spatially varying mechanics of meniscal tissue, and in particular the depth-varying compressive properties.

Due to the lack of information on the depth-varying compressive properties of meniscal tissue and the functional behavior of the meniscal surface, the objective of this study was to characterize and compare depth-varying compressive strains in articular cartilage and

meniscus during unconfined compression. Two-dimensional intra-tissue compressive strain and shear strain distributions were examined for site-matched bovine meniscus and cartilage explants using fluorescence microscopy and digital image correlation. Due to the known variations in ultrastructure and composition through the depth, depth-dependent strain profiles were expected in both tissues.

METHOD

Sample Preparation

Cylindrical cores were isolated with a 6mm biopsy punch from the central portion of the medial meniscus and site-matched tibial articular cartilage (n=12 cores per tissue; Figure 1) of 6 immature bovine stifles (Research 87, Boylston, MA) from 6 different donor animals (1–3 pairs of matched cores per animal). The harvested tissue specimens were frozen and stored at −20C in phosphate buffered saline (PBS, Invitrogen, Carlsbad, California) with protease inhibitors (PIs, Protease Inhibitor Cocktail Set I, EMD Biosciences, San Diego, California). Prior to mechanical testing, the tissue specimens were thawed to room temperature, punched into 4mm diameter cores, and trimmed to 1500μm deep truncated cylinders with intact tibial surfaces using a sliding microtome with a freezing stage. The final thicknesses (surface to base) were 1330 (1280,1380) μm and 1310 (1240, 1380) μm for meniscus and cartilage specimens, respectively. To minimize possible effects of anisotropy on compression results in the meniscal explants, the half-cylinders were cut consistently such that the circumferential collagen bundles ran perpendicular to the cutting surface. Tissues were treated with 1μM ethidium homodimer-1 (EthD-1, Invitrogen, Carlsbad, California) in PBS for 3 hours at room temperature to fluorescently label dead cell nuclei in order to track tissue deformation during compression tests.

Mechanical testing to obtain equilibrium compressive modulus

To obtain the equilibrium compressive modulus of the tissue specimens, 7 matched pairs of the 4mm diameter meniscus and cartilage tissue cylindrical cores were subjected to unconfined compression using a materials testing machine (Instron 5848, Instron, Canton, MA) before being trimmed to half-cylinders. Tissue cores were compressed at a rate of 1μm/s to 5, 10, 15, and 20% nominal applied strain ($\varepsilon_{applied}$) and allowed to stress-relax for 20 minutes at each offset. The equilibrium modulus was determined by linear regression of the relaxed stress against the nominal applied strain.

Mechanical Testing to Investigate Local Strain Distribution

Half-cylindrical tissue cores were subjected to unconfined compression in a custom compression device consisting of a digital depth micrometer and a bath chamber (Figure 3) fitted on an inverted fluorescence microscope (Axiovert 200M, Carl Zeiss MicroImaging, Jena, Germany). The microscope was equipped with ApoTome optical sectioning module that removed out-of-focus information within the tissue sample prior to image acquisition, resulting in cell nuclei visualization of sharper contrast. Tissue specimens were placed in the bath chamber against a glass slide on the bottom of the chamber such that two-dimensional (2D) positions of cell nuclei throughout the tissue could be clearly visualized (Figure 1). After equilibration in PBS + 0.1X PIs for 40 minutes, 10 fluorescence images along the out-of plane direction (Δz = 5μm) were acquired with a Cy3 filter so that the cell nuclei within the tissue could be visualized (Figure 2A). For meniscal specimens, an additional set of fluorescence images was taken using a DAPI filter set with which the secondary fiber network can be visualized due to autofluorescence (Figure 2B). To capture the full depth of the tissue sample, three to four overlapping images were recorded and stitched together using ImageJ (National Institutes of Health, Bethesda, MD). Specimen thickness was determined by averaging three measurements in the stitched image. Samples were manually

compressed with a digital depth micrometer by 5% of the original thickness at ~1μm/s and allowed to stress-relax for 20 minutes before a second image set was acquired. This process was repeated for three additional 5% compression steps up to a total of 20% $\varepsilon_{applied}$. All tissue specimens were imaged with a 10X objective at 0.63μm/pixel.

Tissue Deformation and Engineering Strain Determination

A 2D digital image correlation (DIC) code written in MATLAB (Version 4.6, The Mathworks, Natick, MA) was used to determine tissue deformation by correlating fluorescence images taken at consecutive compression steps. Specifically, square grids of 40 pixels spacing were constructed on the image of an undeformed tissue and Lagrangian displacements (relative to the undeformed image) were obtained by updating the grid locations based on correlations between images of consecutive compression steps. To avoid artifactual influences of the cut surface at the base of the samples, displacement and strain profiles were examined only over the first 1000μm beneath the articular surface of the ~1300μm thick samples.

To produce depth-dependent displacement profiles, displacements were averaged over a lateral width of 600μm at 40 pixels (25.2 μm) spacing through the sample depth for all successfully correlated grid points. To analyze local variations with depth in the compressive engineering strain, displacement profiles over the first 1000μm beneath the articular surface were separately examined for five sequential 200μm-thick segments. Each segment was least squares fitted with a best-fit line, with the slope represented the average engineering strain in the segment. For tissue specimens that exhibited sharp transitions in displacement slope beneath the surface (Figure 3A and B), a bilinear regression was least-squares fitted to the displacement profile to divide the tissue into surface and interior regions. With this bilinear analysis, the average engineering strains in the surface and interior regions could be quantified. An additional parameter, the transition depth, defined the thickness of the surface region at each compression level. The surface to interior equilibrium modulus ratio was given by the ratio of interior to surface engineering strains. Note that while the engineering strain is convenient for describing regionally averaged variations in compression and comparison to the applied nominal strain, it is not a mathematically consistent measure of finite deformation such as the Green's (Lagrangian) strain.

For visual comparisons of 2D strain patterns, in-plane components of the Green's strain tensor were determined under the assumption that out-of-plane shear was negligible. As the DIC algorithm occasionally failed to converge for isolated grid points, uncorrelated regions were interpolated by averaging the neighboring 3X3 grid points. The resulting 2D displacement map was subsequently smoothed over 3X3 grids to generate a continuous displacement field. Partial gradients (u_x, u_y, v_x, v_y) were determined with central differencing and Green's strain components (E_{xx}, E_{yy}, E_{xy}) were obtained.

Statistical Analysis

All statistical analyses were performed using Minitab (Version 15, Minitab, Inc., State College, PA). Repeated measures general linear models (GLMs) were used for all analyses, with animal as a random factor and site nested within animal. For each tissue and for identified subsets of meniscal tissue samples, the local engineering strain was examined with applied strain and segment (layer) as fixed factors. For bilinear fits, regional engineering strains were evaluated with region (surface or interior) and tissue as fixed factors and applied strain as a covariate (including significant interaction terms). Transition depth and modulus ratio (log transformed prior to analysis) were evaluated with tissue as a fixed factor and applied strain as a covariate (including significant interaction terms). Bonferroni's test

was used for pairwise planned comparisons and significance was at $p<0.05$. Values are reported as means with boundaries of 95% confidence intervals (lower limit, upper limit).

RESULTS

The equilibrium compressive moduli for cartilage and meniscus tissue samples (n=7 each) were 447 (363, 531) kPa and 23.6 (17.7, 29.5) kPa, respectively. Note that the unconfined compression modulus of meniscus samples is substantially lower than values reported for the aggregate (confined compression) modulus[13,32], but is consistent with multiple reports of the unconfined compression behavior of meniscal explants[33–35]. Both tissues exhibited depth-varying strain responses to unconfined compression involving increasing local engineering strain with increased applied nominal strain, but the patterns of the responses varied substantially between tissues.

In cartilage samples, the local engineering strain decreased progressively with depth from the tibial surface (Figure 4A). At 5% $\varepsilon_{applied}$, the average local engineering strain was significantly higher in the first layer (0–200μm) than in all deeper layers ($p<0.0001$), with no other significant differences between layers ($p>0.9999$). The mean engineering strain was 3.7 times $\varepsilon_{applied}$ in the first layer (0–200μm) and decreased to 0.28 times $\varepsilon_{applied}$ at 800–1000μm beneath the surface (Figure 4A). As $\varepsilon_{applied}$ increased, the variations with depth in local engineering strain became less abrupt. At $\varepsilon_{applied}$ of 10%, local engineering strains progressively decreased through the first three layers (all comparisons $p \leq 0.0007$), but did not significantly vary among the last three layers (400–1000μm beneath the surface, all comparisons $p \geq 0.89$). At $\varepsilon_{applied}$ of 15% and 20%, local engineering strains progressively decreased through the first four layers beneath the tibial surface (all comparisons $p \leq 0.0005$), but did not significantly differ between the last two layers ($p>0.9999$). At 20% $\varepsilon_{applied}$, the mean engineering strain was 2.3 times $\varepsilon_{applied}$ in the first layer and decreased to 0.35 times $\varepsilon_{applied}$ in the fifth layer beneath the surface.

In contrast, the local engineering strains in meniscus samples increased with depth from the surface (Figure 4B), with an overall pattern that did not vary with increasing applied strain (non-significant interaction). For meniscus samples, the local engineering strains in the first 200μm layer were significantly lower than in the third ($p=0.045$), fourth ($p=0.0024$) or fifth ($p=0.0001$) layer, and the local engineering strain in the second layer was significantly lower than in the fifth layer ($p=0.0071$). At 20% $\varepsilon_{applied}$, the average engineering strain in the first layer was 0.66 times $\varepsilon_{applied}$ and increased to 1.1 times $\varepsilon_{applied}$ in the fourth layer beneath the surface.

While all cartilage explants and half of the meniscus explants exhibited a sharp transition in displacement through the depth of the tissue (Figure 3A and B), some meniscus samples showed no apparent depth-dependent strain response (Figure 3C), with no significant variation in engineering strain among the five 200μm layers in this subset of samples ($p=0.63$). As a result, bilinear regression was used to analyze the subset of meniscal samples with distinct surface and interior responses and the site-matched cartilage samples (n=6/tissue). Engineering strains in all regions increased with $\varepsilon_{applied}$ ($p<0.001$). In cartilage, the surface region engineering strain was 3.04 (2.46, 3.62) times $\varepsilon_{applied}$, while the interior engineering strain was 0.341 (0.304, 0.378) times $\varepsilon_{applied}$ (Figure 5A). On the contrary, meniscus samples had a relatively low surface engineering strain of 0.211 (0.130, 0.292) times $\varepsilon_{applied}$ compared to the interior engineering strain of 1.43 (1.25, 1.61) times $\varepsilon_{applied}$ (Figure 5B). The surface region had substantially higher engineering strains than the interior region in cartilage ($p<0.001$) but substantially lower engineering strains than in the interior in meniscus ($p<0.001$). Comparing tissues, for a given applied strain the surface region had a higher engineering strain in cartilage than in meniscus ($p<0.001$), while the deep region had

a higher engineering strain in meniscus than in cartilage ($p<0.001$). It is important to note that the size of the surface and interior regions changed with applied strain, with the transition depth defining the limit of the surface region. The variation in transition depth with $\varepsilon_{applied}$ was significant ($p<0.001$) and strong for both tissues, but showed opposite trends for cartilage and meniscus (Figure 6), moving deeper into the tissue in cartilage but towards the surface in meniscus with increased applied strain. The ratio of surface to interior equilibrium moduli determined from the strain ratios indicated that the cartilage equilibrium modulus was an order of magnitude higher in the interior region, while the opposite was true for meniscal tissue (Figure 7). The log-transformed modulus ratio increased modestly with $\varepsilon_{applied}$ for cartilage ($p=0.011$, slope = 0.023) and decreased significantly but not substantially with $\varepsilon_{applied}$ for meniscus ($p=0.049$, slope = −0.003).

Two-dimensional Green's strain maps revealed interesting and distinct strain patterns in cartilage and meniscus (Figure 8). Cartilage exhibited relatively uniform compressive and shear strains when comparing regions at the same depth from surface, and the general pattern was consistent across samples. Interestingly, a distinct region of relatively high shear strain was apparent, with a maximum shear strain occurring at approximately 100–250μm beneath the cartilage surface. On the contrary, 2D distributions of all strain components were highly heterogeneous within meniscal samples, particularly in the deep interior regions, and there was substantial variation in the strain patterns between samples, likely reflecting the heterogeneous tissue structure.

DISCUSSION

This study employed a 2D digital image correlation-based strain mapping technique to compare the depth-dependent compressive responses of cartilage and meniscus explants. There are some potential limitations to this approach, particularly due to the lack of deformation measurements in the out-of-plane direction. Although cut carefully while frozen, the thawed samples were not perfectly flat and the unconfined compression configuration did not involve out-of-plane constraints. Minute out-of-plane motion of the tissue is unavoidable especially when large deformation occurs; as a result, the 2D strain measurements might not be sufficient to describe the material's deformation behavior, and some cell nuclei may be "lost" between sequential images due to out-of-plane motion. Creation of the flat surface for visualization inherently requires disruption of the extracellular matrix, which may influence the tissue behavior near the imaged surface. Due to this and the inherent heterogeneity in tissue structure (particularly in meniscal samples), 2D strain field may not fully reflect the overall deformation behavior. Despite these limitations, however, 2D strain-mapping techniques have been used to examine strain fields in many biological tissues[14,28,31,36,37], and the comparison of cartilage and meniscus yields valuable and relevant insights into the behaviors of these two adjacent tissues.

Cartilage and meniscus exhibited fundamentally different depth-varying responses to compression. Consistent with previous findings in articular cartilage[14–18], the local strain in articular cartilage decreased with depth from the tibial surface, indicating a depth-increasing compressive modulus. The relatively compliant surface layer in cartilage has been proposed to play a role in enhancing joint congruity[14]. The strain distributions with depth also depended on the bulk compressive strain applied to the tissue. With increased $\varepsilon_{applied}$, the surface-to-interior modulus ratio increased towards unity, indicating a more even strain distribution through the tissue depth. As $\varepsilon_{applied}$ increased, the apparent transition depth also increased (Figure 5), engaging more tissue in the (relatively) elevated deformation under applied compression.

Half of the meniscus specimens also exhibited a distinct depth-varying compressive response, but with a strikingly different pattern from cartilage. In these meniscus specimens, a large surface region showed relatively little deformation at low $\varepsilon_{applied}$, but the decrease in transition depth implied that the thickness of this surface region decreased rapidly with increased $\varepsilon_{applied}$. The thickness of the low strain surface region showed large variations from sample to sample, ranging from 87.7 to 871μm at 5% $\varepsilon_{applied}$, perhaps reflecting the extremely heterogeneous mesostructure of meniscus. The progressive decrease in surface region thickness with increased $\varepsilon_{applied}$ illustrated that deformation response to compression propagated “inside-out” in meniscal tissue, in sharp contrast to the behavior of cartilage. The rapid expansion of the relatively high strain interior region towards the surface in meniscal tissue might be attributed to structural transformation relating to collagen fiber reorganization. In fact, increasing buckling of the secondary collagen fibers and shearing/reorganization of the circumferential collagen fiber bundles with increasing $\varepsilon_{applied}$ were observed in fluorescence images of meniscus explants (Figure 2B). These internal structural transformations may allow the tissue to redistribute compressive strain and adjust to changes in loading while maintaining surface contour and integrity, contributing to the maintenance of joint congruity in a very different manner from articular cartilage. Overall, while strain patterns in cartilage samples were quite consistent, the 2D strain patterns observed in meniscus appeared to be more complex and variable both within and between samples, which could be attributed to the non-uniform organization of collagen fiber structures. This is consistent with earlier observations of substantial intra- and inter-sample heterogeneity in strain fields for porcine meniscal tissue under circumferential tension[31]. Interestingly, while a distinct layer (ranging from approximately 100–250μm thick) was observed in the fluorescence images of meniscal tissue, possibly indicating the location of the superficial and lamellar layers (Figure 2B), there was no obvious relationship between compressive strain transition depth and the thickness of this surface layer.

Contrary to articular cartilage, few reports have addressed the depth-varying compressive properties in the meniscus. Proctor et al.[13] performed confined compression tests on 1mm-thick cylindrical cores obtained from the femoral surface (surface) and from interior (deep) of mature bovine medial menisci. The average aggregate modulus (determined via confined compression tests) from central medial menisci was approximately 400kPa and did not vary significantly between the surface and deep layer. Similarly, a preliminary study from our laboratory using consecutive 2mm thick samples of immature bovine meniscus found no significant differences with depth in equilibrium or dynamic unconfined compression moduli or in dynamic shear moduli[38]. In contrast, results from the current study indicated that the surface region of meniscus has a significantly higher compressive modulus than the interior of the tissue. While animal age and loading protocol (unconfined vs. confined compression) differed among these studies, the approach taken in the present study allowed examination of the tissue deformation response with much finer spatial resolution, leading to new insights into depth-varying meniscal function.

Although applied strain was in the axial direction only, lateral expansion and structural transformation of the tissue during unconfined compression induced internal shear in the tissue specimens. Maps of E_{xy} (shear component of Green’s strain) revealed a characteristic maximum shear band at 100–250μm beneath the articular surface in cartilage specimens (Figure 8). The observation of sub-surface maximum shear band is consistent with the findings in shear testing conducted by Buckley et al.[27,28], showing minimum shear modulus at 50–250 μm below the articular surface at the boundary of the superficial zone. This result might be a consequence of local buckling of collagen fibers at the transition zone separating the superficial zone which is populated with tangential collagen fibrils and the middle zone which is characterized by randomly oriented fibril[28]. In contrast, no characteristic depth-varying shear pattern was observed in meniscus specimens. In general,

meniscus exhibited highly heterogeneous shear strain, likely reflecting material inhomogeneity and structural transformations such as collagen fiber buckling within the tissue. It should be noted that in meniscal specimens that exhibited low surface compressive strain, the shear strain in the surface region was minimal, indicating little deformation in surface region in contrast to the interior of the tissue.

The results of this study showed that cartilage and meniscal tissue have very distinct depth-dependent responses to compressive deformation. Although the geometry of the tissue specimens as well as the unconfined compression loading protocol may not accurately reflect actual strain distributions within the tissue during physiological loading conditions, these findings provide important baseline knowledge of the intrinsic depth-varying mechanical properties of meniscus. While the functional role of the circumferential collagen fibers in sustaining tensile hoop stress within the meniscus during compression has been well described in literature, the role of the extensive secondary fiber network (referred to as tie fibers in most earlier studies) under compression has received little attention. Skaggs et al.[39] showed that these secondary fibers, referred to as ‘radial tie fibers’, increased tensile modulus of the tissue and suggested its role in preventing excessive extrusion of the meniscus during compression by constraining the main fiber bundles. For the first time, we were also able to observe internal structural organization of the collagen bundles and buckling of the secondary fiber network within the meniscal tissue during unconfined compression, suggesting possible role of the secondary fiber network in compressive load bearing. These tests were by necessity conducted in the absence of normal tension in the circumferential fiber bundles, resulting in greater compliance than would be found physiologically. Nevertheless, these observations indicate that the matrix surrounding the circumferential fibers is functionally important and merits further investigation. In vitro, the initial stages of meniscal tissue degeneration involve proteoglycan catabolism within this secondary matrix, producing a drastic reduction in macroscopic compressive and shear properties[33]. Similar processes during early stages of meniscal degeneration may impair the normal biomechanical functions of the meniscus resulting in increased deformation and movement of the meniscus and alterations in load transfer, possibly contributing to a cascade of degenerative responses in both meniscus and cartilage.

Acknowledgments

This study was supported by an NIH grant (NIAMS R01AR052861) and an NSF Graduate Research Fellowship. We would like to thank Dr. Robert Sah, Dr. Won Bae, and Quynhhoa Nguyen for technical advice and An Nguyen for technical assistance with equipment development.

Supported by National Institutes of Health (NIAMS) grant R01AR052861 and a National Science Foundation Graduate Research Fellowship

References

1. Mow, VC.; Gu, WY.; Chen, FH. Structure and function of articular cartilage and meniscus. In: Mow, VC.; Huiskes, R., editors. Basic orthopaedic biomechanics & mechanobiology. Philadelphia: Lippincott Williams & Wilkins; 2005. p. 181-258.
2. Andriacchi TP, Mundermann A, Smith RL, Alexander EJ, Dyrby CO, Koo S. A framework for the in vivo pathomechanics of osteoarthritis at the knee. Ann Biomed Eng. 2004; 32:447–457. [PubMed: 15095819]
3. Fithian DC, Kelly MA, Mow VC. Material properties and structure-function relationships in the menisci. Clin Orthop Relat Res. 1990:19–31. [PubMed: 2406069]
4. Akizuki S, Mow VC, Muller F, Pita JC, Howell DS, Manicourt DH. Tensile properties of human knee joint cartilage.1. Influence of ionic conditions, weight bearing and fibrillation on the tensile modulus. Journal of Orthopaedic Research. 1986; 4:379–392. [PubMed: 3783297]

5. Maroudas, A. Physiochemical properties of articular cartilage. In: Freeman, MAR., editor. Adult articular cartilage. Tunbridge Wells: Pitman Medical; 1979. p. 215-290.
6. Petersen W, Tillmann B. Collagenous fibril texture of the human knee joint menisci. Anat Embryol (Berl). 1998; 197:317–324. [PubMed: 9565324]
7. Valiyaveettil M, Mort JS, McDevitt CA. The concentration, gene expression, and spatial distribution of aggrecan in canine articular cartilage, meniscus, and anterior and posterior cruciate ligaments: a new molecular distinction between hyaline cartilage and fibrocartilage in the knee joint. Connect Tissue Res. 2005; 46:83–91. [PubMed: 16019418]
8. Kambic HE, McDevitt CA. Spatial organization of types I and II collagen in the canine meniscus. Journal of Orthopaedic Research. 2005; 23:142–149. [PubMed: 15607886]
9. Vanderploeg, EJ. Mechanical Engineering, vol. Doctor of Philosophy. Atlanta: Georgia Institute of Technology; 2006. Mechanotransduction in Engineered Cartilaginous Tissues: In Vitro Oscillatory Tensile Loading; p. 28-53.
10. Chevrier A, Nelea M, Hurtig MB, Hoemann CD, Buschmann MD. Meniscus structure in human, sheep, and rabbit for animal models of meniscus repair. J Orthop Res. 2009; 27:1197–1203. [PubMed: 19242978]
11. Leslie BW, Gardner DL, McGeough JA, Moran RS. Anisotropic response of the human knee joint meniscus to unconfined compression. Proc Inst Mech Eng H. 2000; 214:631–635. [PubMed: 11201410]
12. Zhu W, Chern KY, Mow VC. Anisotropic viscoelastic shear properties of bovine meniscus. Clin Orthop Relat Res. 1994:34–45. [PubMed: 8070209]
13. Proctor CS, Schmidt MB, Whipple RR, Kelly MA, Mow VC. Material properties of the normal medial bovine meniscus. J Orthop Res. 1989; 7:771–782. [PubMed: 2677284]
14. Schinagl RM, Gurskis D, Chen AC, Sah RL. Depth-dependent confined compression modulus of full-thickness bovine articular cartilage. J Orthop Res. 1997; 15:499–506. [PubMed: 9379258]
15. Erne OK, Reid JB, Ehmke LW, Sommers MB, Madey SM, Bottlang M. Depth-dependent strain of patellofemoral articular cartilage in unconfined compression. Journal of Biomechanics. 2005; 38:667–672. [PubMed: 15713286]
16. Wang CC, Deng JM, Ateshian GA, Hung CT. An automated approach for direct measurement of two-dimensional strain distributions within articular cartilage under unconfined compression. J Biomech Eng. 2002; 124:557–567. [PubMed: 12405599]
17. Chen SS, Falcovitz YH, Schneiderman R, Maroudas A, Sah RL. Depth-dependent compressive properties of normal aged human femoral head articular cartilage: relationship to fixed charge density. Osteoarthritis and Cartilage. 2001; 9:561–569. [PubMed: 11520170]
18. Canal CE, Hung CT, Ateshian GA. Two-dimensional strain fields on the cross-section of the bovine humeral head under contact loading. J Biomech. 2008; 41:3145–3151. [PubMed: 18952212]
19. Klein TJ, Chaudhry M, Bae WC, Sah RL. Depth-dependent biomechanical and biochemical properties of fetal, newborn, and tissue-engineered articular cartilage. J Biomech. 2007; 40:182–190. [PubMed: 16387310]
20. Bae WC, Lewis CW, Levenston ME, Sah RL. Indentation testing of human articular cartilage: effects of probe tip geometry and indentation depth on intra-tissue strain. J Biomech. 2006; 39:1039–1047. [PubMed: 16549094]
21. Gratz KR, Wong BL, Bae WC, Sah RL. The effects of focal articular defects on cartilage contact mechanics. J Orthop Res. 2009; 27:584–592. [PubMed: 18979528]
22. Gratz KR, Wong BL, Bae WC, Sah RL. The effects of focal articular defects on intra-tissue strains in the surrounding and opposing cartilage. Biorheology. 2008; 45:193–207. [PubMed: 18836224]
23. Choi JB, Youn I, Cao L, Leddy HA, Gilchrist CL, Setton LA, et al. Zonal changes in the three-dimensional morphology of the chondron under compression: the relationship among cellular, pericellular, and extracellular deformation in articular cartilage. J Biomech. 2007; 40:2596–2603. [PubMed: 17397851]
24. Guterl CC, Gardner TR, Rajan V, Ahmad CS, Hung CT, Ateshian GA. Two-dimensional strain fields on the cross-section of the human patellofemoral joint under physiological loading. J Biomech. 2009; 42:1275–1281. [PubMed: 19433326]

25. Wong BL, Bae WC, Gratz KR, Sah RL. Shear deformation kinematics during cartilage articulation: effect of lubrication, degeneration, and stress relaxation. Mol Cell Biomech. 2008; 5:197–206. [PubMed: 18751528]
26. Wong BL, Bae WC, Chun J, Gratz KR, Lotz M, Sah RL. Biomechanics of cartilage articulation: effects of lubrication and degeneration on shear deformation. Arthritis Rheum. 2008; 58:2065–2074. [PubMed: 18576324]
27. Buckley MR, Bergou AJ, Fouchard J, Bonassar LJ, Cohen I. High-resolution spatial mapping of shear properties in cartilage. J Biomech. 2010; 43:796–800. [PubMed: 19896130]
28. Buckley MR, Gleghorn JP, Bonassar LJ, Cohen I. Mapping the depth dependence of shear properties in articular cartilage. Journal of Biomechanics. 2008; 41:2430–2437. [PubMed: 18619596]
29. Ho MM, Kelly TA, Guo XE, Ateshian GA, Hung CT. Spatially varying material properties of the rat caudal intervertebral disc. Spine. 2006; 31:E486–493. [PubMed: 16816748]
30. Michalek AJ, Buckley MR, Bonassar LJ, Cohen I, Iatridis JC. Measurement of local strains in intervertebral disc anulus fibrosus tissue under dynamic shear: contributions of matrix fiber orientation and elastin content. J Biomech. 2009; 42:2279–2285. [PubMed: 19664773]
31. Upton ML, Gilchrist CL, Guilak F, Setton LA. Transfer of macroscale tissue strain to microscale cell regions in the deformed meniscus. Biophys J. 2008; 95:2116–2124. [PubMed: 18487290]
32. Sweigart MA, Athanasiou KA. Toward tissue engineering of the knee meniscus. Tissue Eng. 2001; 7:111–129. [PubMed: 11304448]
33. Wilson CG, Vanderploeg EJ, Zuo F, Sandy JD, Levenston ME. Aggrecanolysis and in vitro matrix degradation in the immature bovine meniscus: mechanisms and functional implications. Arthritis Res Ther. 2009; 11:R173. [PubMed: 19919704]
34. Bursac P, Arnoczky S, York A. Dynamic compressive behavior of human meniscus correlates with its extra-cellular matrix composition. Biorheology. 2009; 46:227–237. [PubMed: 19581729]
35. Chia HN, Hull ML. Compressive moduli of the human medial meniscus in the axial and radial directions at equilibrium and at a physiological strain rate. J Orthop Res. 2008; 26:951–956. [PubMed: 18271010]
36. Doehring TC, Kahelin M, Vesely I. Direct measurement of nonuniform large deformations in soft tissues during uniaxial extension. J Biomech Eng. 2009; 131:061001. [PubMed: 19449955]
37. Bay BK. Texture correlation: a method for the measurement of detailed strain distributions within trabecular bone. J Orthop Res. 1995; 13:258–267. [PubMed: 7722763]
38. Nishimuta, JF.; Nguyen, AM.; Levenston, ME. Depth-Dependent Mechanical Properties in Articular Cartilage and Meniscal Fibrocartilage. 55th Annual Meeting of the Orthopaedic Research Society; 2009.
39. Skaggs DL, Warden WH, Mow VC. Radial tie fibers influence the tensile properties of the bovine medial meniscus. Journal of Orthopaedic Research. 1994; 12:176–185. [PubMed: 8164089]

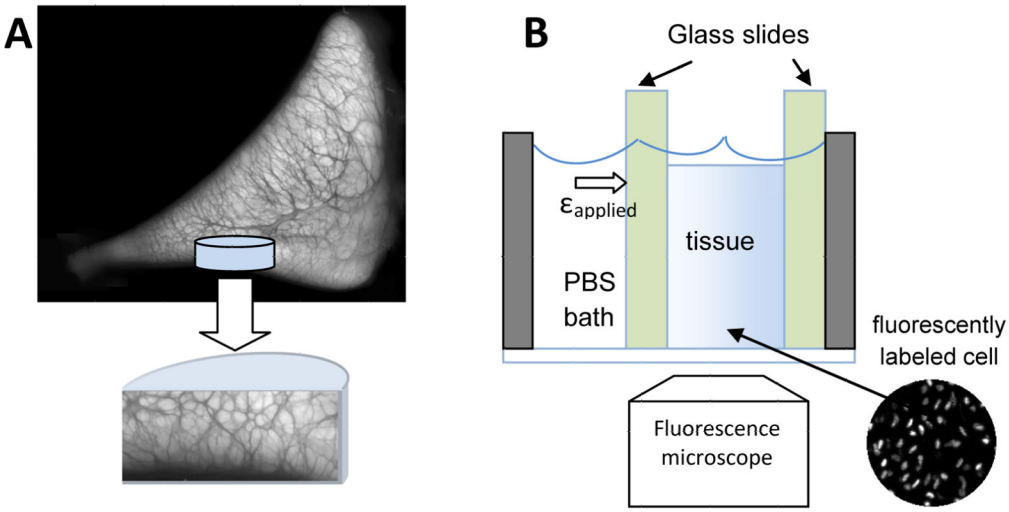

Figure 1.

Schematics of (**A**) a tissue core harvested from medial meniscus at the tibial surface and (**B**) experimental setup of the compression test. Semi-cylindrical tissue cores were sandwiched between two glass slides and deformation profile as indicated by fluorescently labeled cell nuclei were recorded after each stress-relaxation step. The darker regions in the cross-sectional image demonstrate the extensive, interconnected secondary network surrounding the circumferential collagen fibers (lighter regions) in meniscal tissue.

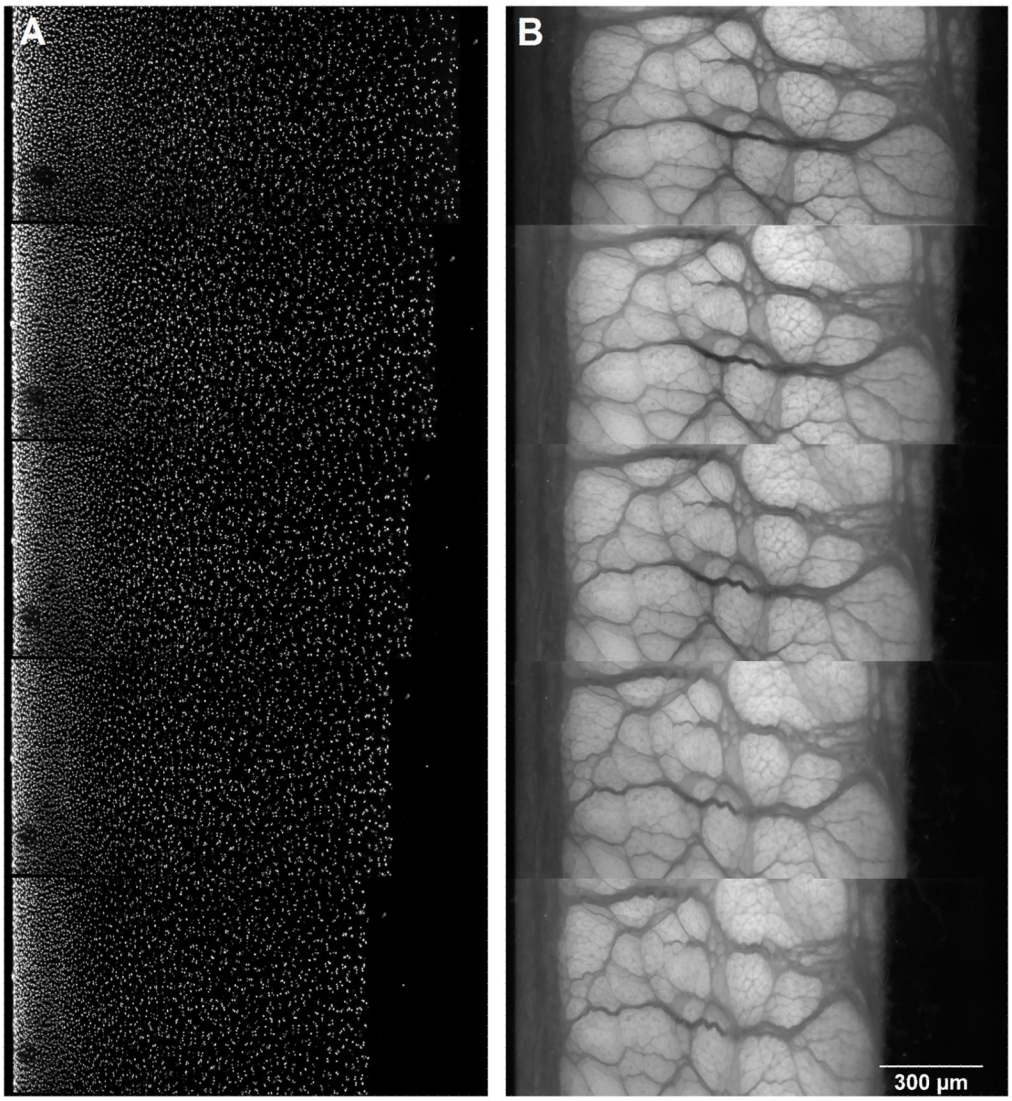

Figure 2.
Fluorescence images of (**A**) cartilage showing cell nuclei and (**B**) meniscus showing the secondary fiber network in the uncompressed state (top) and at 5%, 10, 15, and 20% applied strain (bottom).

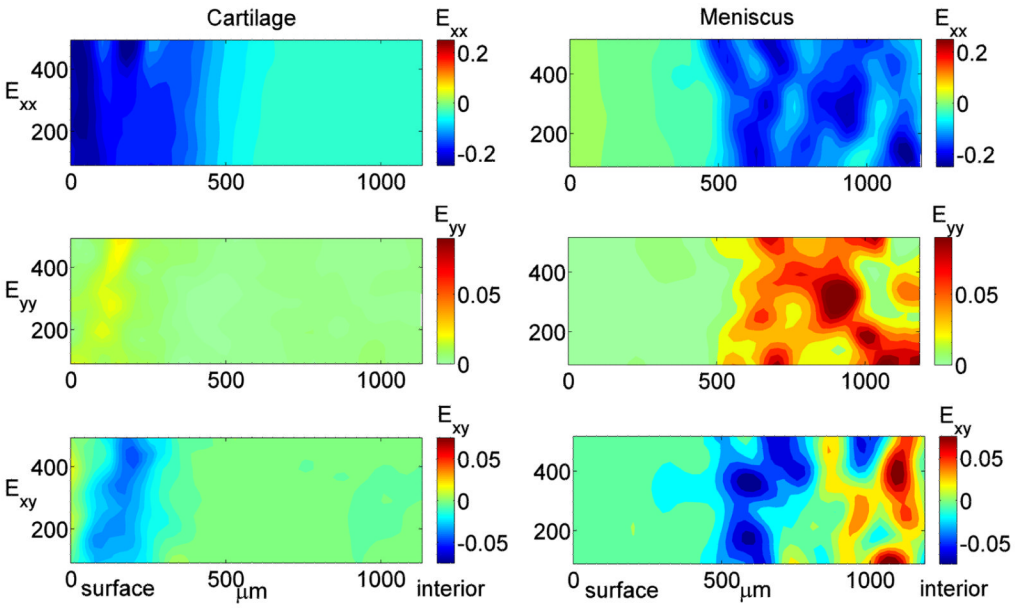

Figure 3.

Representative axial displacements (mean with 95% confidence interval, n=17–192 successfully correlated grid points at each depth) of (A) cartilage and (B,C) meniscus samples at 5, 10, 15, 20% $\varepsilon_{applied}$. Solid lines connect the mean displacements for each $\varepsilon_{applied}$, and dotted lines (A,B) represent bilinear regressions fit to the average displacements at each $\varepsilon_{applied}$. All cartilage and half of the meniscal samples exhibited clear transitions in nominal strains (A,B), while the remaining meniscus samples had no abrupt changes with depth (C).

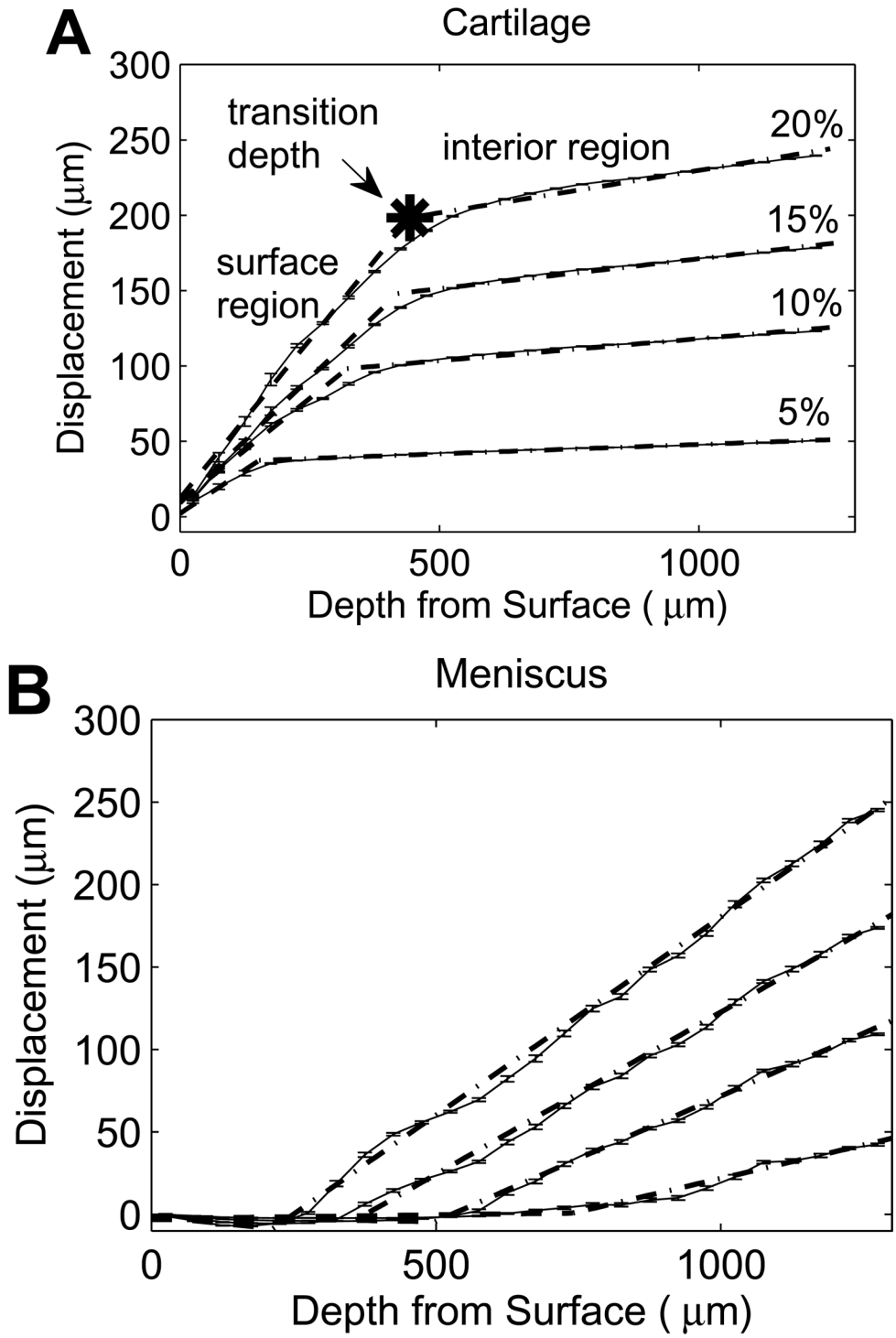

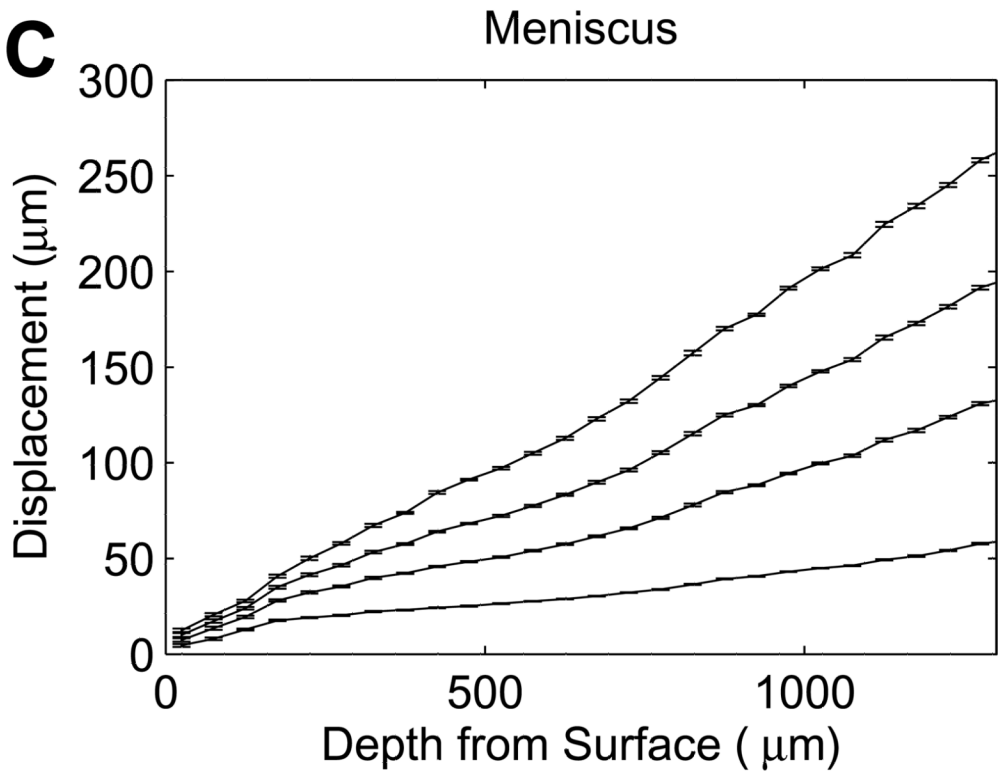

Figure 4.
Compressive engineering strains in the first five 200-μm tissue layers beneath the tibial surface in (**A**) cartilage and (**B**) meniscus (mean with 95% confidence interval, n=12 samples).

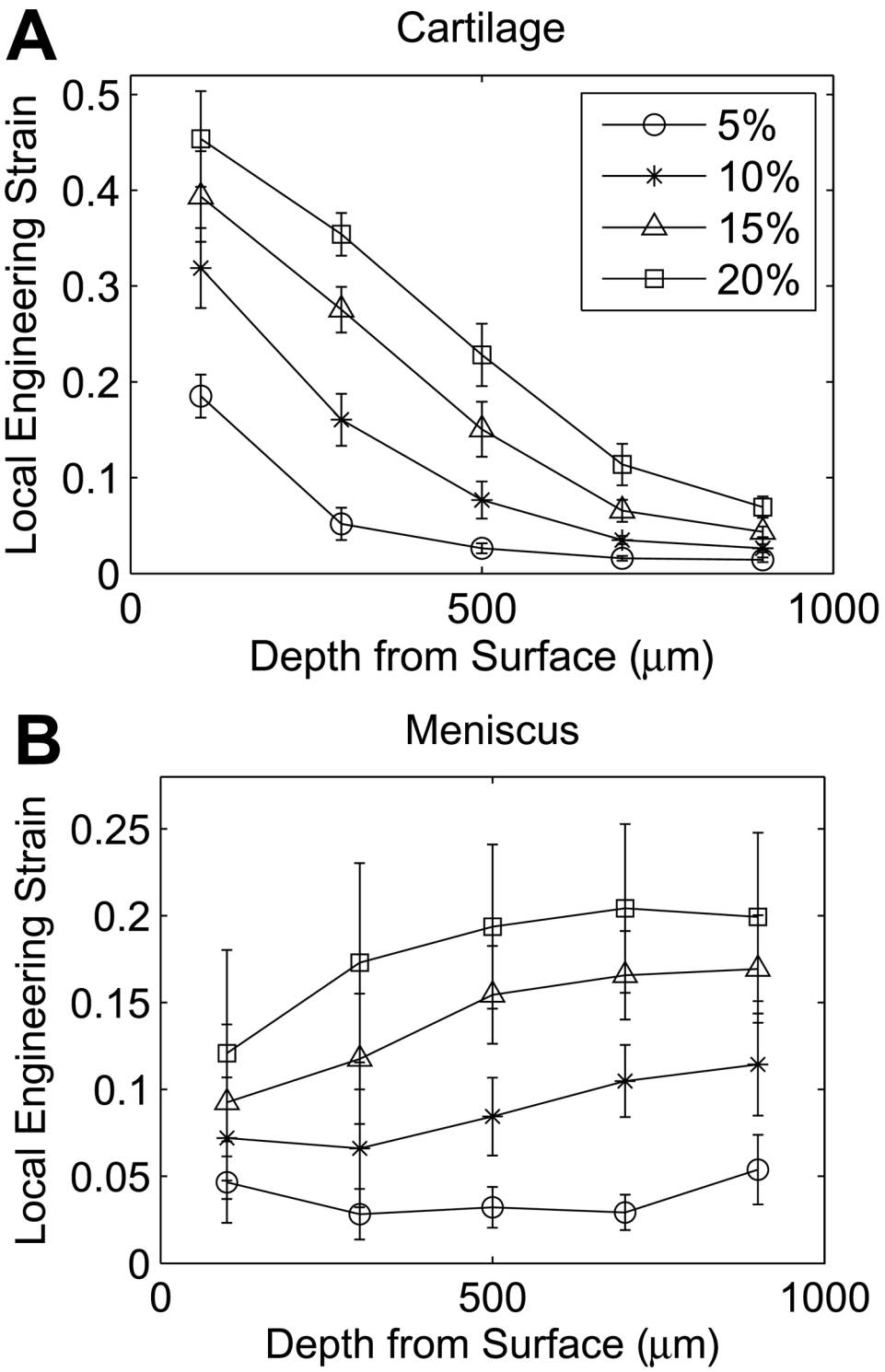

Figure 5.
Variations in local nominal strains with increased applied strain in matched (**A**) cartilage (left) and (**B**) meniscus samples for pairs including meniscal explants displaying distinct strain transitions (mean with 95% confidence interval, n=6 samples).

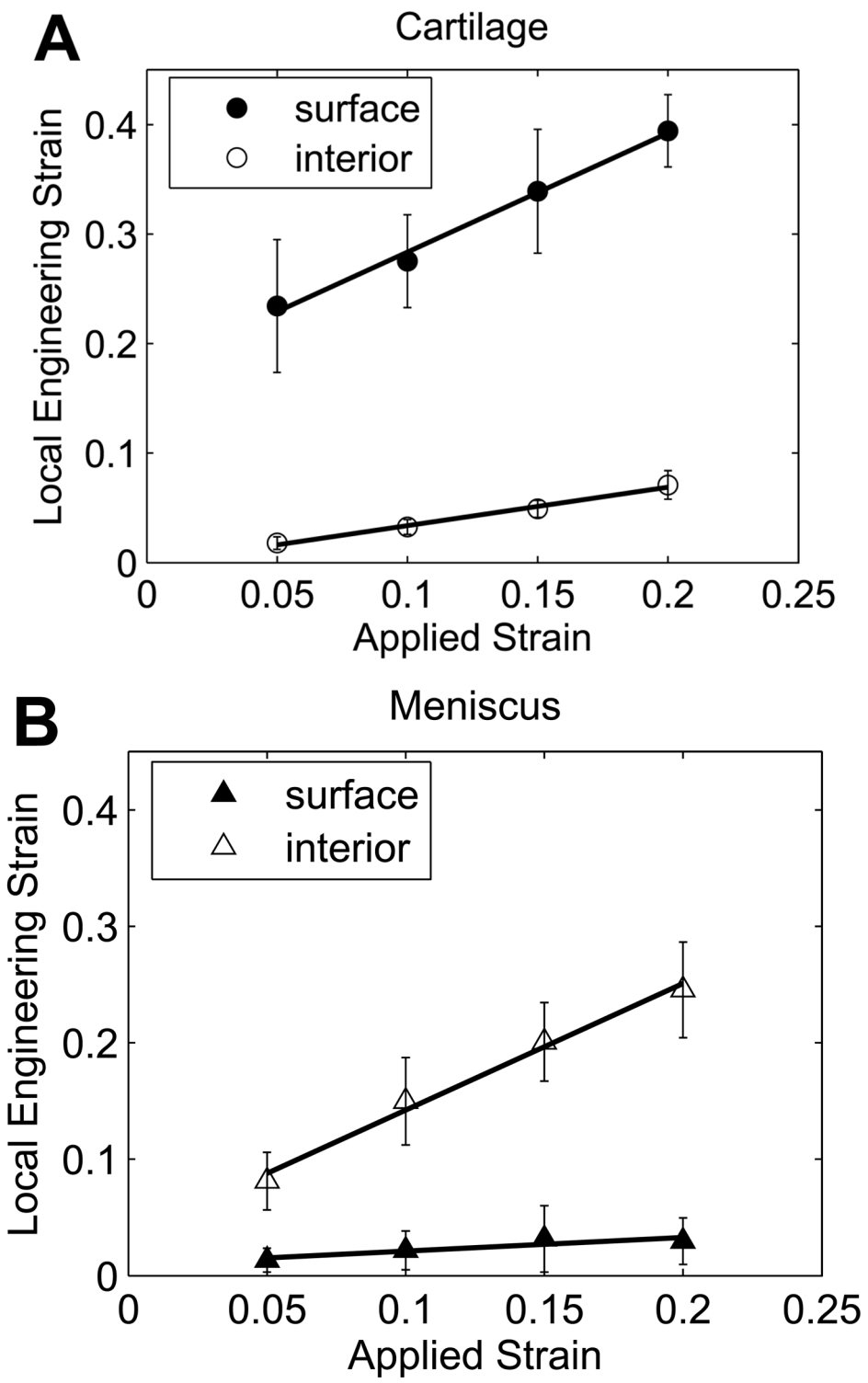

Figure 6.
Transition depth as a function of $\varepsilon_{applied}$ for pairs including meniscal explants displaying distinct strain transitions (mean with 95% confidence interval, n=6 samples).

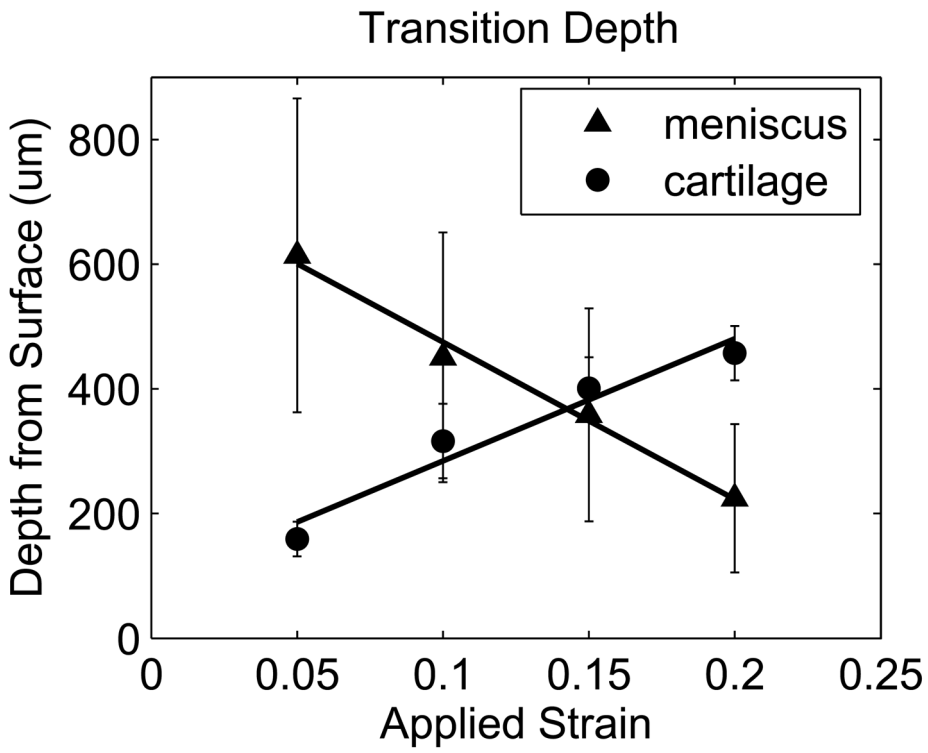

Figure 7.
Modulus ratio as a function of $\varepsilon_{applied}$ for pairs including meniscal explants displaying distinct strain transitions (mean with 95% confidence interval, n=6 samples).

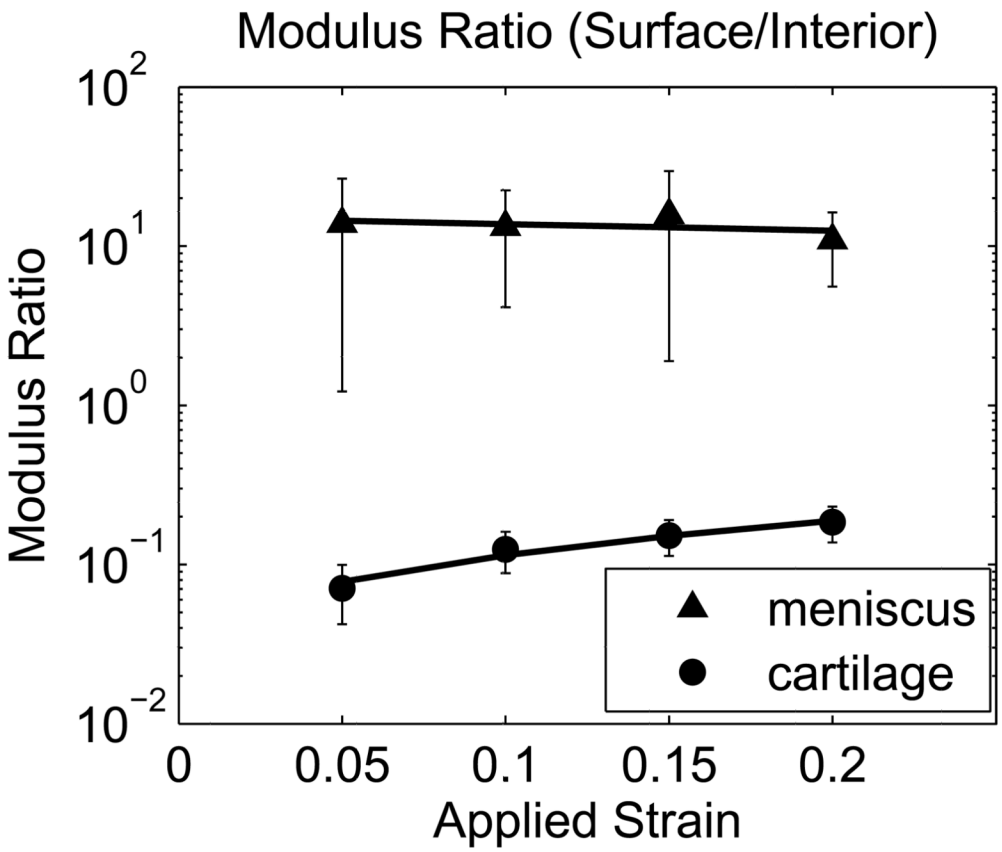

Figure 8.

Representative contour maps of 2D Green's strain components: normal strain in the direction of (E_{xx}) and transverse to (E_{yy}) the applied compression and shear strain (E_{xy}) for cartilage (left) and meniscus (right) at 10% $\varepsilon_{applied}$. Cartilage strain patterns were qualitatively consistent across multiple samples, while meniscal strain patterns were highly variable both within and between samples.